

# Chelation Crosslinking of Biodegradable Elastomers

Ying Chen, Paula G. Miller, Xiaochu Ding, Chelsea E. T. Stowell, Katie M. Kelly, and Yadong Wang\*

Widely present in nature and in manufactured goods, elastomers are network polymers typically crosslinked by strong covalent bonds. Elastomers crosslinked by weak bonds usually exhibit more plastic deformation. Here, chelation as a mechanism to produce biodegradable elastomers is reported. Polycondensation of sebacic acid, 1,3-propanediol, and a Schiff-base (2-[(2-hydroxyphenyl) methylene]amino]-1,3-propanediol) forms a block copolymer that binds several biologically relevant metal ions. Chelation offers a unique advantage unseen in conventional elastomer design because one ligand binds multiple metal ions, yielding bonds of different strengths. Therefore, one polymeric ligand coordinated with different metal ions produces elastomers with vastly different characteristics. Mixing different metal ions in one polymer offers another degree of control on material properties. The density of the ligands in the block copolymer further regulates the mechanical properties. Moreover, a murine model reveals that Fe<sup>3+</sup> crosslinked foam displays higher compatibility with subcutaneous tissues than the widely used biomaterial—polycaprolactone. The implantation sites restore to their normal architecture with little fibrosis upon degradation of the implants. The versatility of chelation-based design has already shown promise in hydrogels and highly stretchy nondegradable polymers. The biodegradable elastomers reported here would enable new materials and new possibilities in biomedicine and beyond.

Elastomer is a polymer with a glass transition temperature ( $T_g$ ) lower than room temperature and with low plastic deformability.<sup>[1]</sup> Elastic recoil makes an elastomer essential for maintaining functions of natural tissues including heart, lung, blood vessels, skin, and man-made structures such as gaskets, hoses, and tires. Covalent bonds link random coiled polymers into elastomers such as elastin, resilin, silicone, and vulcanized rubber.<sup>[2]</sup> Weak bonds perform same task in polyurethanes, polyamide, and polyvinyl chloride.<sup>[3]</sup> Each of these elastomers has its own chemistry that dictates a specific bond to crosslink into a network. Thus, the design must be tailored to each polymer

Dr. Y. Chen, P. G. Miller, Dr. X. Ding, Dr. C. E. T. Stowell, Prof. Y. Wang  
 Meinig School of Biomedical Engineering, College of Engineering  
 Cornell University  
 277 Kimball Hall, 134 Hollister Drive, Ithaca, NY 14853, USA  
 E-mail: yw839@cornell.edu

Dr. K. M. Kelly  
 Department of Biomedical Sciences  
 College of Veterinary Medicine  
 Cornell University  
 Ithaca, NY 14853, USA

 The ORCID identification number(s) for the author(s) of this article can be found under <https://doi.org/10.1002/adma.202003761>.

DOI: 10.1002/adma.202003761

and each resultant polymer will have a specific set of properties. This makes elastomer design a laborious process and limits the versatility and range of properties of the resultant material. We set out to overcome this using chelation bonds, weaker than covalent but stronger than typical weak bonds used in crosslinking. This design is highly versatile in that one ligand binds different kinds of metal ions. The resultant coordination bonds will have different strengths, leading to different mechanical properties and biodegradability.

Our polymer design focuses on three factors. First, the type of coordination bonds: When a metal-ligand interaction involves multiple bonds, it becomes a chelation bond and is stronger. We use chelation bonds to have a wider range of bond strength and mechanical properties in the resultant polymers. Second, the type of ligand: The ligand is effectively half a salen. It provides two coordination bonds so that two and three of the pendant groups on the polymer chains create a tetradeятate and hexadентate

ligand respectively for the appropriate metal ions to nucleate the crosslinks (Figure 1). Third, polymer backbone and metal ions: With a focus on the potential biomedical applications, we choose degradable ester bonds and biologically relevant metal ions: Mg<sup>2+</sup>, Ca<sup>2+</sup>, Fe<sup>3+</sup>, Cu<sup>2+</sup>, Zn<sup>2+</sup>, and Co<sup>2+</sup>.<sup>[4]</sup> The diacid monomer is sebacic acid because of its known biocompatibility.<sup>[5]</sup> The diols are a Schiff-base ligand (2-[(2-hydroxyphenyl)methylene]amino]-1,3-propanediol, HPA) and 1, 3-propanediol. The former derives from serinol, offering good biocompatibility.<sup>[6]</sup> 1, 3-propanediol is a common food additive, pharmaceutical excipient, and has demonstrated safety in vivo.<sup>[7]</sup>

The identity of the metal ions, metal/ligand ratio and ligand density significantly impact mechanical properties of the resultant polymer. The biocompatibility and biodegradability of Fe<sup>3+</sup> crosslinked elastomers were examined using human umbilical vein endothelial cells (HUVECs) and subcutaneous implantation in mice. In summary, this simple crosslinking mechanism affords polymers with a wide range of mechanical properties and excellent biocompatibility.

The Schiff-base ligand HPA (Figure 1A), bearing two hydroxyl groups and one phenol, is synthesized by a simple condensation (Figures S1–S3, Supporting Information). We prepared a series of biodegradable elastomers crosslinkable by metal ions. Polycondensation of 1, 3-propanediol, HPA, and sebacic acid

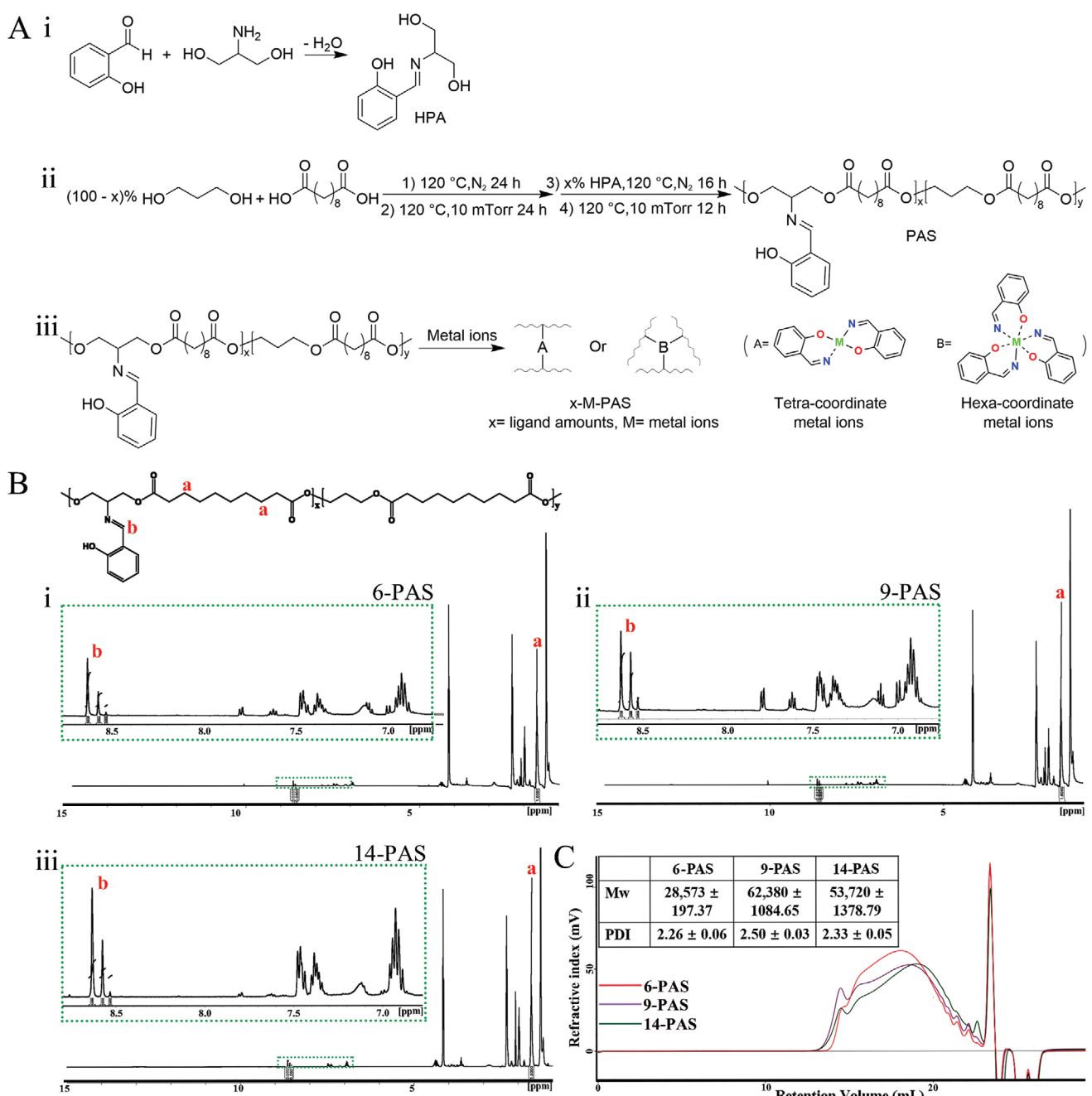


**Figure 1.** Material design and polymer characterization. A) Synthesis of 2-[(2-hydroxyphenyl)methylene]amino-1,3-propanediol (HPA), poly(propanediol-HPA-sebacate) (PAS), and M-PAS elastomers. B) Structural formula of PAS and  $^1\text{H}$  NMR (500 Hz) spectra of 6-PAS (i), 9-PAS (ii), and 14-PAS (iii) polymers in acetone-d<sub>6</sub>. Ratio of integrations of H<sub>b</sub> and H<sub>a</sub> determines actual ligand amounts. C) Gel permeation chromatography of 6-, 9-, and 14-PAS. Inset: weight-average molecular weight ( $M_w$ ) and polydispersity (PDI). Data represent mean  $\pm$  SD,  $n = 3$ .

produces poly(propanediol-*co*-(hydroxyphenylmethylen)amino-propanediol sebacate) (PAS). Hydroxyl groups of 1,3-propanediol and HPA are converted into the ester bonds of the polyester backbone, leaving the phenolic oxygen and Schiff-base as pendant groups (Figure 1A). PAS polymers containing three different densities of ligands: 6%, 9%, and 14%, are synthesized (denoted as 6-, 9-, and 14-PAS, respectively) by adjusting molar percentage of HPA in the diols (Figure 1B; Figures S4 and S5, Supporting Information). The  $M_w$  of the

6-, 9-, and 14-PAS are 28 573, 62 380, and 53 720 Da, respectively (Figure 1C). The salicylaldimine side groups (ligand) are pendant on these polymer backbones that could influence polymer chain packing, mobility, crystallization, and consequently the thermal properties. All PAS polymers demonstrate three thermal events: glass transition ( $T_g$ ), melting ( $T_m$ ), and crystallization ( $T_c$ ) in differential scanning calorimetry (DSC), indicating they are semicrystalline materials (Figure S6, Supporting Information).

Metal coordination bond is found in natural<sup>[8]</sup> and synthetic materials.<sup>[9]</sup> Poly(dimethylsiloxane) polymer grafted with 2,6-pyridinedicarboxamide ligands has been crosslinked by Fe<sup>3+</sup> to prepare a highly stretchable self-healing polymer.<sup>[10]</sup> Most recently, a Cu(II)-dimethylglyoxime-urethane-complex-based polyurethane elastomer (Cu-DOU-CPU) with synergistic triple dynamic bonds has been developed and has shown superb mechanical properties.<sup>[11]</sup> The coordination bonds impart versatility to polymer network because we can design a ligand to bind different types of metal ions, providing additional control to polymer properties such as stiffness, toughness, and viscoelastic dissipation. Here, two or three of the ligands will chelate tetra- and hexa-coordinate metal ions leading to crosslinking of polymer chains. Immediately after adding a metal ion, for example, Fe<sup>3+</sup>, the PAS solution gels, indicating crosslinking. Chelation bonds should be reversible in the presence of a competing ligand. The gel returns to a solution within 1 min of adding ethylenediaminetetraacetic acid (EDTA), an excellent ligand for many transition metals (Movie S1, supporting information). Polymers are large molecules, with lower mobility and solvent diffusivity than small molecules. Therefore, after mixing polymers and metal ions in solution, the crosslinked polymers (M-PAS) are heated at 150 °C for 8 h at 30 mTorr to remove solvents. To test if heating introduces additional crosslinks, we subject PAS alone to identical heating protocols. PAS is stable up to 283 °C with no noticeable decomposition, as revealed by TGA (Figure S7, Supporting Information). PAS heated at 150 °C and 30 mTorr for 8 h dissolves well in organic solvents such as acetone, unlike the crosslinked M-PAS (Figure S8A, Supporting Information). <sup>1</sup>H NMR spectra of 14-PAS before and after heat treatment are virtually identical (Figure S8B, Supporting Information). Thus, heating alone causes no appreciable crosslinking. In Fourier-transformed infrared (FTIR) spectrum of 9-Fe-PAS, shift of  $\nu(C=N)$  mode from 1625 cm<sup>-1</sup> in the free ligand to 1590 cm<sup>-1</sup> indicates bond formation through imino nitrogen atom,<sup>[12]</sup> further corroborating chelation between salicylaldimine of PAS and iron (Figure S9, Supporting Information). Using dynamic bonds such as hydrogen bonds is another versatile strategy to establish crosslinks in elastomers.<sup>[13]</sup> The chelation-bond crosslinking reported here adds a new tool to create elastomers with a focus on biodegradability and biocompatibility.

As indicated by DSC results, PAS is amorphous at 37 °C. Uncrosslinked PAS polymer can be processed into various shapes because it melts into a liquid and dissolves in common organic solvents such as acetone, tetrahydrofuran, isopropanol, chloroform and hexafluoroisopropanol. We prepared M-PAS into films, foams and porous tubes. Using 9-Cu-PAS as an example, the films and foams exhibit excellent elastic recoil (Figure 2A; Movies S2 and S3, Supporting Information). The 9-Cu-PAS porous tube has a porosity of approximately 65% (Micro-CT, Figure S10, Supporting Information) and can be twisted repeatedly without deformation.

The ester backbone of M-PAS degrades by hydrolysis. We use an accelerated, supraphysiological in vitro degradation in a PBS solution containing  $60 \times 10^{-3}$  M NaOH (pH = 12.63) to investigate degradation of 14-M-PAS films. After 48 h under agitation at 37 °C, 14-M-PAS films crosslinked by Mg<sup>2+</sup>, Ca<sup>2+</sup>, Fe<sup>3+</sup>, Co<sup>2+</sup>, Cu<sup>2+</sup>, and Zn<sup>2+</sup> degrade gradually with the remaining mass of 13%, 55%, 34%, 71%, 74%, and 22%, respectively (Figure 2B).

Degradation rate of M-PAS elastomers varies with metal ions, relating to their different metal-ligand chelating strength. The most durable among these, 14-Cu-PAS, hydrolyzes 5.83 times more slowly than the fastest variant crosslinked by Mg<sup>2+</sup>.

Coordination bonds are reversible in that another chelator can compete for metal ions and break the bond. A  $10 \times 10^{-3}$  M EDTA solution in DMF/H<sub>2</sub>O (1/1, v/v) extracts metal ions from the 6-M-PAS elastomers within 72 h under agitation at 70 °C, accompanied by appreciable polymer degradation (Figure 2C). After EDTA extraction, the mass remaining (%) for 6-M-PAS films ranges from 14% to 80%, depending on metal ions. This supports the necessity of metal-ligand crosslinking in elastomer formation and suggests that different strength of chelation bonds determines stability of the crosslinked polymer. Faster degradation of 6-M-PAS in the presence of EDTA demonstrates that metal coordination bonds are holding the polymer network together and that the crosslinking can be reversed by another ligand. This offers a new way to control polymer degradation.

We examine the cytocompatibility by culturing HUVECs on coatings of the elastomers. Poly(*ε*-caprolactone) (PCL) has a long history as a biomaterial and is familiar to many researchers in the field. Thus, commercially sourced PCL ( $M_n = 80\,000$  Da) serves as a control. We choose Fe<sup>3+</sup> because among the ions used, 14-Fe-PAS exhibits a medium degradation rate. HUVECs maintain typical endothelial morphology and display the same proliferating and spreading behavior on both 14-Fe-PAS and PCL coatings with few dead cells (Figure 2D). MTT assay demonstrates the same metabolic activity on 14-Fe-PAS and PCL. These results suggest that 14-Fe-PAS is at least as cytocompatible as PCL in vitro.

We chose 9-Fe-PAS as a representative of M-PAS elastomers to examine the feasibility of controlling mechanical properties by the number of crosslinks. Molar ratios of ligand in 9-PAS to Fe<sup>3+</sup> ranges from 1 to 6. In UV-vis spectra (Figure 3A,i; Figure S13, Supporting Information), absorption at 327 nm of 9-PAS represents the  $\pi \rightarrow \pi^*$  transition, and formation of 9-Fe-PAS shifts the  $\pi \rightarrow \pi^*$  transition from 327 to 328 nm (ligand/Fe<sup>3+</sup> = 1), 326 nm (ligand/Fe<sup>3+</sup> = 2) and 325 nm (ligand/Fe<sup>3+</sup> = 3, 4, 5, and 6). Peak shifts of ligand/Fe<sup>3+</sup> ratios of 1 and 2 are smaller than those of others, implying there are excessive free ligands. Absorption shift reaches maximum at ligand/Fe<sup>3+</sup> of 3. It remains the same beyond 3 because Fe<sup>3+</sup> is hexa-coordinate and no more chelation bond forms with increasing availability of ligands. Bands at 350–400 nm of 9-Fe-PAS with different ligand/Fe<sup>3+</sup> ratios are due to charge-transfer in the complex, and the weak broad bands at 450–650 nm are due to d → d transition of Fe<sup>3+</sup> ion, both are absent in 9-PAS. Tensile stress curves of 9-Fe-PAS films show that decreasing Fe<sup>3+</sup> amount results in softer and more stretchable films (Figure 3A, ii; Figure S14, Supporting Information). When molar ratio of ligand/metal increases from 2 to 6, the strain at break increases from  $144 \pm 9.20\%$  to  $394 \pm 42.6\%$ , the ultimate tensile strength (UTS) decreases from  $1127 \pm 57.86$  to  $552 \pm 55.59$  kPa, the Young's modulus (E) decreases from  $2125 \pm 190.25$  to  $674 \pm 121.34$  kPa and the toughness remains at around  $1000 \text{ kJ m}^{-3}$ . This is because fewer crosslinkers lead to longer polymer chains between the crosslinks, resulting in a more stretchy elastomer.<sup>[14]</sup>

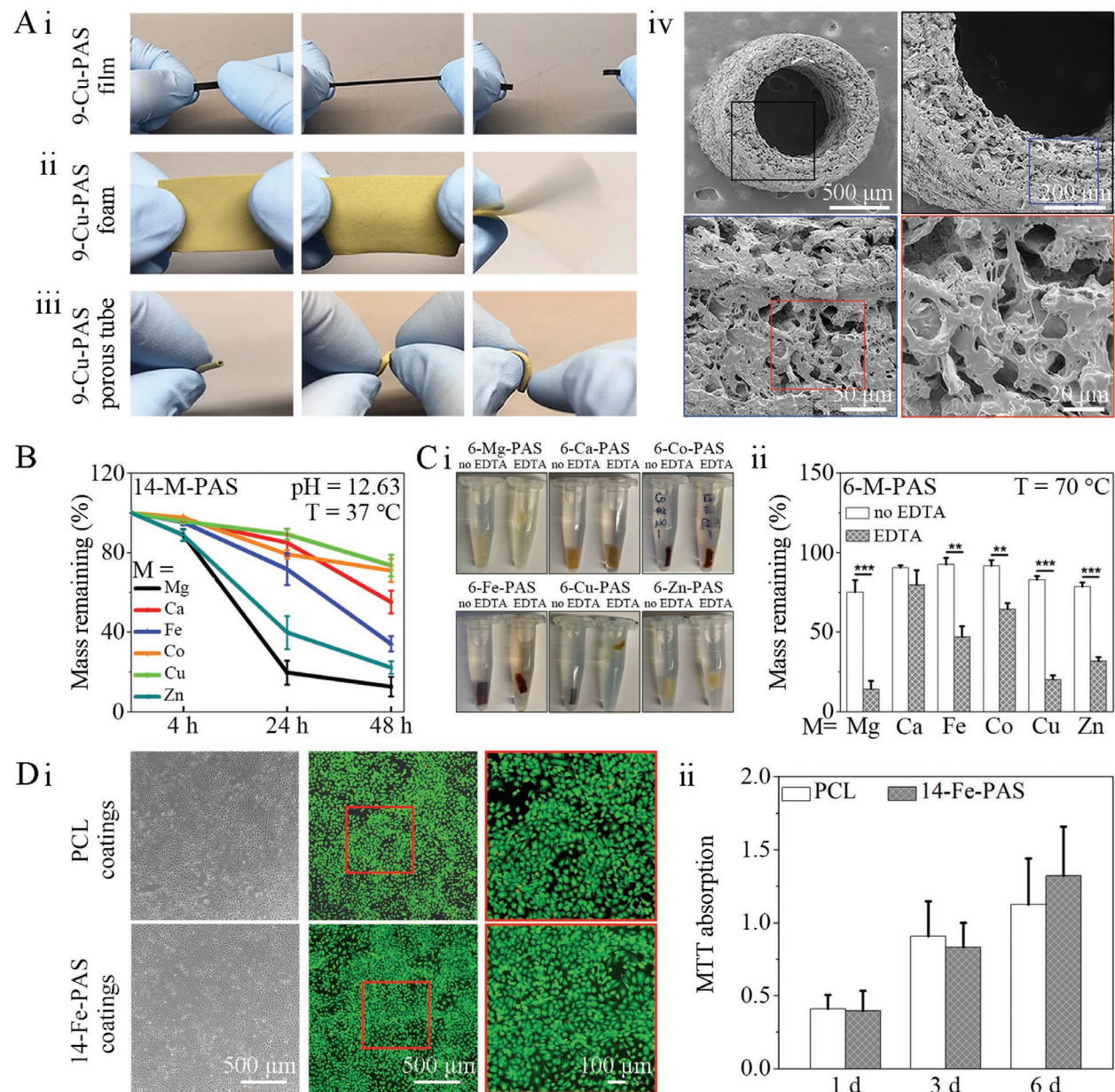


**Figure 2.** Versatility, degradation, and cytocompatibility of M-PAS. A) 9-Cu-PAS in film (i), foam (ii), and porous tube (iii). A typical M-PAS is highly elastic. The shape recovers rapidly after release of external force. Videos are in the Supporting Information. SEM images of cross-sections of porous 9-Cu-PAS tube (iv). B) Degradation of 14-M-PAS in a basic solution. C) Photographs (i) and degradation (ii) of 6-M-PAS films in an EDTA solution. D) Cell morphology, live/dead staining (i), and metabolic activity (ii) of HUVECs after 6 d culture on 14-Fe-PAS and PCL coatings. Data represent mean  $\pm$  SD,  $n = 3$ . \*\*,  $p < 0.01$ ; \*\*\*,  $p < 0.001$ .

Co-PAS films with varied ligand density are prepared and used for tensile tests. To simplify, ligand/metal ratio is fixed at 2. Tensile tests on the three variants of Co-PAS reveal stress-strain curve characteristics of elastomeric materials<sup>[15]</sup> with a wide range of mechanical properties: a 3.30-fold range of strain, 6.95-fold of stress, and 8.55-fold of modulus (Figure 3B; Figure S15, Supporting Information). With an increase of ligand density from 6% to 14%, the UTS increases from  $316 \pm 67$  to  $2200 \pm 201$  kPa, Young's modulus increases from  $0.33 \pm 0.20$  to  $2.82 \pm 0.50$  MPa, and the strain at break decreases from  $772 \pm 171\%$  to  $234 \pm 45\%$ , consistent with an increase of crosslinking density. The same trend holds for the other metals investigated (will be published

later). Therefore, with a certain metal ion, altering ligand density of PAS controls the mechanical properties.

With a given ligand density, different metals have different chelation bond strengths, offering an additional means to control the mechanical properties of M-PAS. Using 14-M-PAS as an example, among the six metal ions tested,  $\text{Ca}^{2+}$  forms the toughest elastomer with a strain of break at  $515.00 \pm 29.02\%$ , UTS of  $1493.68 \pm 461.11$  kPa, modulus of  $722 \pm 297.46$  kPa, and toughness of  $3538 \pm 1028.56$  kJ m<sup>-3</sup>. 14-Fe-PAS has the smallest strain at  $132.11 \pm 21.62\%$ , highest UTS at  $2289.86 \pm 99.14$  kPa and highest Young's modulus at  $3823 \pm 237.30$  kPa (Figure 3C; Figure S16, Supporting Information). Comparison among these

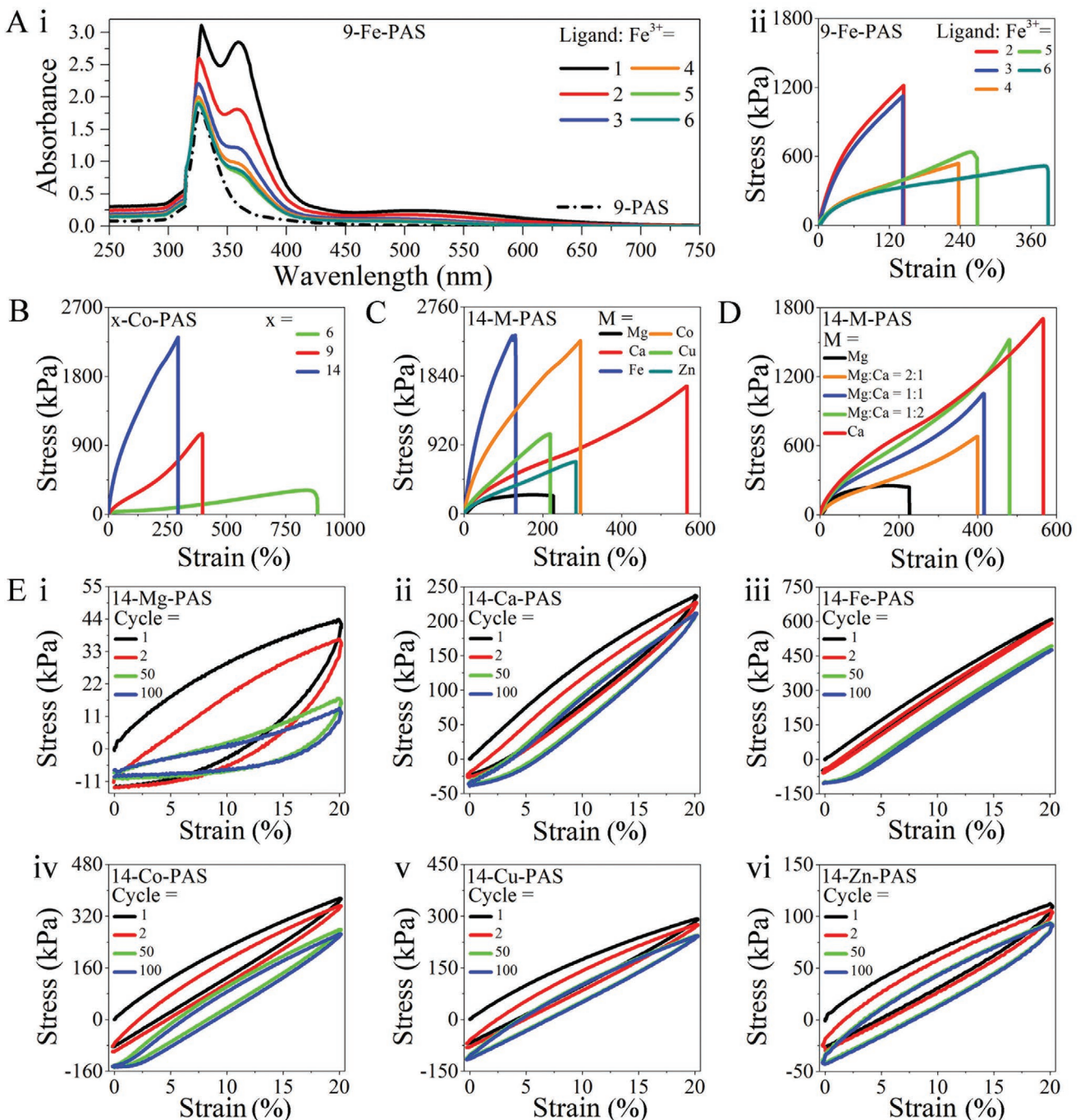


**Figure 3.** Control mechanical property of M-PAS by ligand/metal ratio, ligand density, and metal ion types. A) UV-vis spectra of 9-Fe-PAS with different ligand/metal ratios (i). Stress–strain curves of 9-Fe-PAS films with different metal/ligand ratios (ii). B) Stress–strain curves of  $x$ -Co-PAS,  $x = 6, 9$ , and  $14$ . C) Stress–strain curves of 14-M-PAS films with different metal ions.  $M = \text{Mg}^{2+}$  (i),  $\text{Ca}^{2+}$  (ii),  $\text{Fe}^{3+}$  (iii),  $\text{Co}^{2+}$  (iv),  $\text{Cu}^{2+}$  (v), and  $\text{Zn}^{2+}$  (vi). D) Stress–strain curves of 14-Mg-Ca-PAS films with different  $\text{Mg}^{2+}/\text{Ca}^{2+}$  ratios. E) Hysteresis tests of 14-M-PAS films with different metal ions.  $M = \text{Mg}^{2+}$  (i),  $\text{Ca}^{2+}$  (ii),  $\text{Fe}^{3+}$  (iii),  $\text{Co}^{2+}$  (iv),  $\text{Cu}^{2+}$  (v), and  $\text{Zn}^{2+}$  (vi).

metal ions is crucial for future selection of metal ions to obtain elastomers with specific mechanical properties to meet the demand of a specific application. An advantage of crosslinking via coordination bond is the possibility of using a mixture of metal ions in the same polymer network. We mix  $\text{Mg}^{2+}$  with  $\text{Ca}^{2+}$  in molar ratios of 2:1, 1:1, and 1:2 to prepare the 14-Mg-Ca-PAS elastomers (Figure 3D; Figure S17, Supporting Information).

$\text{Mg}^{2+}$  and  $\text{Ca}^{2+}$  yield the weakest and toughest polymers respectively among the six types of 14-M-PAS. The mechanical property of the 14-Mg-Ca-PAS films is controlled by the metal ion ratio within the boundary set by 14-Mg-PAS and 14-Ca-PAS, enabling fine tuning of the mechanics by mixing metal ions.

The ability to recover from mechanical deformation is key to the function of an elastomer in a mechanically dynamic

environment.<sup>[16]</sup> We performed hysteresis tests on 14-M-PAS films. The strain to 20% (Figure 3E) is equal to or greater than what many soft tissues such as ligaments and arteries typically experience.<sup>[17]</sup> All films can undergo cyclic loading for at least 100 cycles without rupture. The hysteresis test reveals that metal ions determine the elastic recoil of 14-M-PAS. Mg crosslinked polymer shows pronounced hysteresis loops with reduced stress as cycles increase, which indicates energy dissipation from bond breakage.<sup>[18]</sup> In contrast, polymers crosslinked by other metal ions show small hysteresis loops, indicating little damage occurs during cyclic loading. Fe crosslinked polymer is the most elastic among those tested, reflecting strong chelation of Fe<sup>3+</sup> to PAS. The elasticity is attributed to the rapid dynamic association and dissociation of chelation bonds between metal

ions and salicylaldimine side groups of PAS under deformation. This dissipates the loading stress efficiently enabling the high capacity of M-PAS to tolerate deformations.

Using 14-Fe-PAS as an example, we evaluate its biocompatibility via a subcutaneous implantation model in mice with PCL ( $M_n = 80,000$  Da) as a control. All polymer foams have a similar pore structure with porosity of ~62% (Figure S19, Supporting Information). One 14-Fe-PAS foam and one PCL foam of identical size are implanted symmetrically into back of the same mouse (Figure S20, Supporting Information). All mice survive without malignancy, infections or abscesses at implantation sites (Figure 4; Figures S21 and S22, Supporting Information). For 14-Fe-PAS foams, H&E staining reveals cells only at surfaces with no sign of degradation at day 4. After 14 d, cells

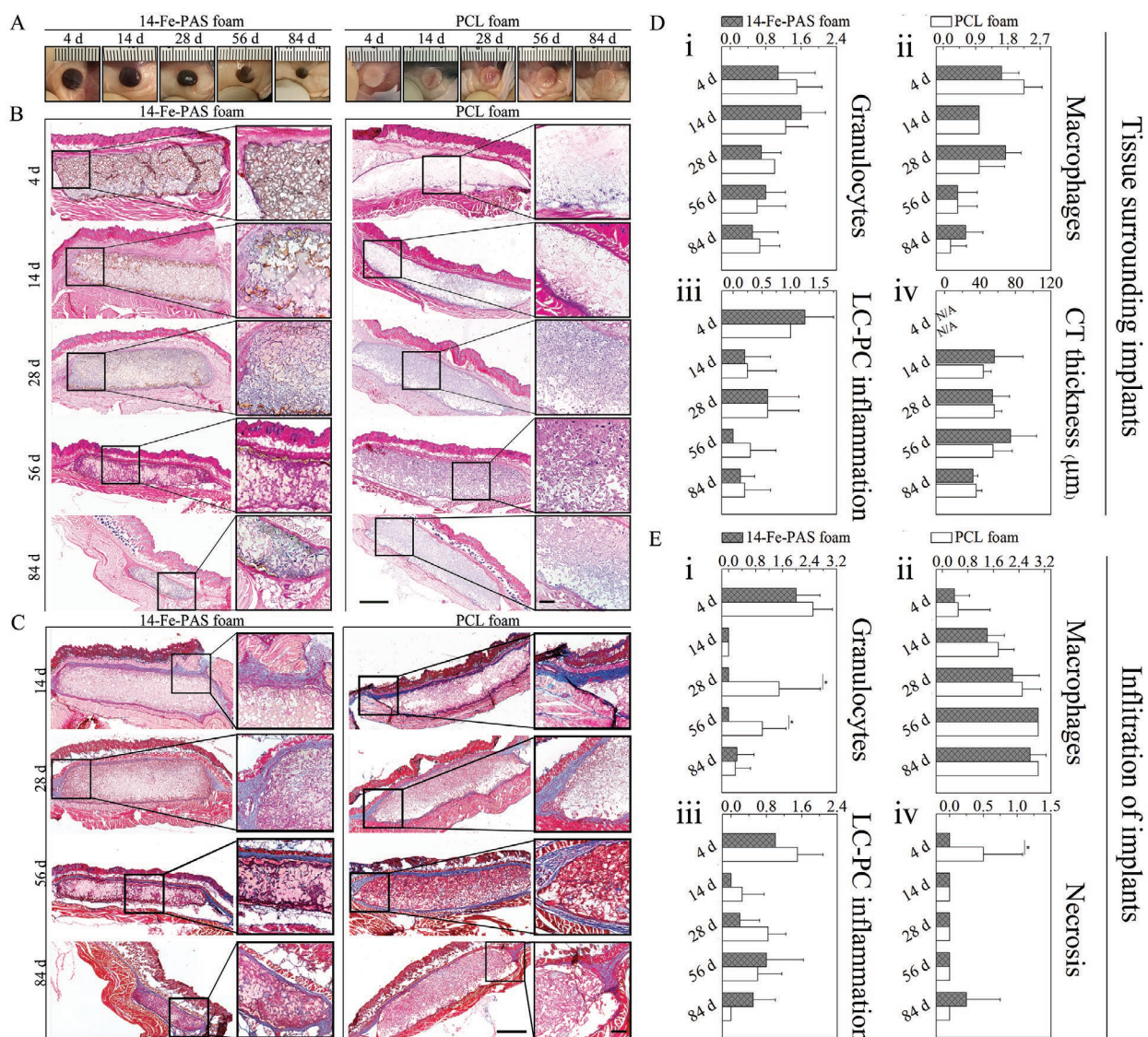


**Figure 4.** Subcutaneous implantation of 14-Fe-PAS foams in mice. A) Gross appearance of 14-Fe-PAS and PCL foams after being implanted for 4, 14, 28, 56, and 84 d. Unit of ruler: mm. B,C) Photomicroscopy images of H&E and MTS staining for cross-sections of the implants. Slides are obtained by sectioning at center of each implant. Scale bars for low magnification: 1.0 mm; high magnification: 200 μm. D) Granulocytes (i), macrophages (ii), LC-PC inflammation (iii), and CT thickness (iv) in tissue surrounding implants. E) Granulocytes (i), macrophages (ii), LC-PC inflammation (iii), and necrosis (iv) within implants. LC-PC = lymphoplasmacytic, CT = connective tissue. Data represent mean ± SD, n = 5. Significant difference: \*, p < 0.05.

infiltrate deeper and implants show visible rounding at edge, likely because of degradation. On day 28, cells infiltrate entire implants with fibrovascular tissues and degradation of the bulk starts, as indicated by the reduced presence of polymers. However, the implants maintain their original shape, indicative of mechanical integrity. Histological analysis suggests that most of the 14-Fe-PAS has degraded by day 84. The control PCL foams show cells infiltration after 14 d. The bulk of PCL foams starts a limited degradation afterward. PCL implants retain their shape with little dimensional change after 84 d. 14-Fe-PAS degrades faster than PCL in vivo and exhibits a 4.67 times higher degradation rate than PCL in vitro (Figure S23, Supporting Information).

Tissues around both 14-Fe-PAS and PCL implants show mild adverse responses such as inflammation and fibrosis (Figure 4; Figures S21,S22,S24–S26, Supporting Information). Inflammatory cells recruit in surface areas of all implants at day 4 because of a nonspecific inflammatory response to the implants,<sup>[19]</sup> and then migrate into and proliferate inside the implants. Throughout the observation window, number of granulocytes in tissues surrounding 14-Fe-PAS and PCL implants shows no difference, while there are a significantly higher number of granulocytes inside PCL than those inside 14-Fe-PAS at 28 and 56 d. Macrophages, key mediators of inflammation and wound healing, show a slightly higher presence in surrounding tissues of PCL than in 14-Fe-PAS at day 4. There are larger numbers of macrophages inside PCL implants than 14-Fe-PAS at all time points. Fibroblasts play an important role in wound healing after implantation.<sup>[20]</sup> Number of fibroblasts in tissues surrounding 14-Fe-PAS at day 56 is significantly higher than that of PCL, while the infiltrating fibroblasts inside implants are at a similar level in both groups. Lymphoplasmacytic inflammation, as a type of chronic inflammation consisting of lymphocytes and plasma cells,<sup>[21]</sup> is also scored but no difference shows in 14-Fe-PAS and PCL. Overall, PCL shows slightly stronger inflammation than 14-Fe-PAS. 14-Fe-PAS degrades faster than PCL, presenting a higher concentration of degradation products in microenvironment of the implant site. Thus, inflammatory responses to PCL would likely be stronger if degradation of PCL matches that of 14-Fe-PAS. Collagen deposition is part of wound healing response to an implant. Fibrous capsules surround 14-Fe-PAS and PCL foam from day 14 onward. Capsule thickness is similar for both materials at all time points. Moreover, the fibrillar connective tissues in the surrounding tissue and collagen within the implants show no difference in 14-Fe-PAS and PCL. Overall, 14-Fe-PAS induces a milder inflammatory response than PCL in the subcutaneous environment.

In summary, this report demonstrates the versatility of metal chelation bonds in crosslinking biodegradable elastomers. A wide range of mechanical properties can be obtained by using different types of metal ions, mixing different metal ions in one polymer, metal to ligand ratios, and ligand density in the polymers. The biocompatibility of the elastomers matches that of PCL, opening promising new avenues for elastomer development for improved soft tissue reconstruction and regeneration. In particular, the high degree of elastic recoil would be advantageous in tissues experiencing large deformations, such as ligaments, blood vessels, skin, lung, kidney, and heart. The crosslinking mechanism enables many new

research possibilities, for example, mixing different types of metal ions, adding a spacer between the ligand and main chain, and explore other types of ligands. Furthermore, metal ions can impart biological functions after integration into polymers.<sup>[22]</sup> These would enable new material properties previously unseen and new opportunities in multiple fields.

## Supporting Information

Supporting Information is available from the Wiley Online Library or from the author.

## Acknowledgements

This work was supported by a startup fund from Cornell University. This work uses the Cornell Center for Materials Research Shared Facilities which are supported through the NSF MRSEC program (DMR-1719875) and the Cornell University NMR Facility, supported by the NSF MRI award CHE-1531632. All work with live animals followed a protocol (protocol # 2017-0118) approved by the Cornell University Institutional Animal Care and Use Committee. Human umbilical vein endothelial cells (HUVECs) (C2519A) were obtained from Lonza, MD, USA.

## Conflict of Interest

The authors declare no conflict of interest.

## Keywords

biocompatibility, biodegradable elastomers, metal chelation crosslinking

Received: June 1, 2020

Revised: August 19, 2020

Published online: September 22, 2020

- [1] S. K. De, J. R. White, *Rubber Technologist's Handbook*, Smithers Rapra Publishing, Akron, OH, USA **2001**.
- [2] L. Engle, K. Wagener, *J. Macromol. Sci., Part C: Polym. Rev.* **1993**, *33*, 239.
- [3] a) X. Ding, Y. Wang, *J. Mater. Chem. B* **2017**, *5*, 887; b) M. Chanda, *Plastics Technology Handbook*, CRC Press, Boca Raton, FL, USA **2017**.
- [4] a) R. Kozyraki, O. Cases, *Biochimie* **2013**, *95*, 1002; b) S. Gupta, *MOL Bioorg. Org. Chem.* **2018**, *2*, 221.
- [5] a) G. Liu, B. Hinch, A. D. Beavis, *J. Biol. Chem.* **1996**, *271*, 25338; b) A. Grego, G. Mingrone, *Clin. Nutr.* **1995**, *14*, 143.
- [6] B. Andreeßen, A. Steinbüchel, *AMB Express* **2011**, *1*, 12.
- [7] a) R. Gingell, J. B. Kirkpatrick, D. R. Steup, *Int. J. Toxicol.* **2000**, *19*, 27; b) R. S. Scott, S. R. Frame, P. E. Ross, S. E. Loveless, G. L. Kennedy, *Inhalation Toxicol.* **2005**, *17*, 487.
- [8] M. J. Harrington, A. Masic, N. Holten-Andersen, J. H. Waite, P. Fratzl, *Science* **2010**, *328*, 216.
- [9] a) N. Iwamoto, B. Eichinger, N. Andersen, *Rubber Chem. Technol.* **1984**, *57*, 944; b) J.-Y. Sun, X. Zhao, W. R. Illeperuma, O. Chaudhuri, K. H. Oh, D. J. Mooney, J. J. Vlassak, Z. Suo, *Nature* **2012**, *489*, 133; c) Y.-L. Rao, A. Chortos, R. Pfattner, F. Lissel, Y.-C. Chiu, V. Feig, J. Xu, T. Kurosawa, X. Gu, C. Wang, M. He, J. W. Chung, Z. Bao, *J. Am. Chem. Soc.* **2016**, *138*, 6020; d) D. E. Fullenkamp, L. He, D. G. Barrett, W. R. Burghardt, P. B. Messersmith, *Macromolecules* **2013**, *46*, 1167; e) P. Calvo-Marzal, M. P. Delaney, J. T. Auletta, T. Pan,

- N. M. Perri, L. M. Weiland, D. H. Waldeck, W. W. Clark, T. Y. Meyer, *ACS Macro Lett.* **2012**, *1*, 204; f) J. M. Pollino, M. Weck, *Chem. Soc. Rev.* **2005**, *34*, 193.
- [10] C.-H. Li, C. Wang, C. Keplinger, J.-L. Zuo, L. Jin, Y. Sun, P. Zheng, Y. Cao, F. Lissel, C. Linder, X.-Z. You, Z. Bao, *Nat. Chem.* **2016**, *8*, 618.
- [11] a) Z. Liu, L. Zhang, Q. Guan, Y. Guo, J. Lou, D. Lei, S. Wang, S. Chen, L. Sun, H. Xuan, E. M. Jeffries, C. He, F. Qing, Z. You, *Adv. Funct. Mater.* **2019**, *29*, 1901058; b) L. Zhang, Z. Liu, X. Wu, Q. Guan, S. Chen, L. Sun, Y. Guo, S. Wang, J. Song, E. M. Jeffries, C. He, F. Qing, X. BAO, Z. You, *Adv. Mater.* **2019**, *31*, 1901402.
- [12] a) M. Haque, K.-E. Zahan, L. A. Banu, S. Islam, M. S. Islam, *Bioinorg. Chem. Appl.* **2015**, *2015*, 1; b) R. Radford, A. Abedi, *J. Appl. Chem. Res.* **2015**, *9*, 59.
- [13] a) R. Du, Z. Xu, C. Zhu, Y. Jiang, H. Yan, H. C. Wu, O. Vardoulis, Y. Cai, X. Zhu, Z. Bao, Q. Zhang, X. Jia, *Adv. Funct. Mater.* **2020**, *30*, 1907139; b) E. C. Davidson, A. Kotikian, S. Li, J. Aizenberg, J. A. Lewis, *Adv. Mater.* **2020**, *32*, 1905682; c) Y. Chen, A. M. Kushner, G. A. Williams, Z. Guan, *Nat. Chem.* **2012**, *4*, 467.
- [14] R. Dash, M. Foston, A. J. Ragauskas, *Carbohydr. Polym.* **2013**, *91*, 638.
- [15] M. A. Meyers, K. K. Chawla, *Mechanical Behavior of Materials*, Cambridge University Press, Cambridge, UK **2008**.
- [16] W. Wu, R. A. Allen, Y. Wang, *Nat. Med.* **2012**, *18*, 1148.
- [17] R. A. Allen, W. Wu, M. Yao, D. Dutta, X. Duan, T. N. Bachman, H. C. Champion, D. B. Stolz, A. M. Robertson, K. Kim, J. S. Isenberg, Y. Wang, *Biomaterials* **2014**, *35*, 165.
- [18] X. Hu, M. Vatankhah-Varnoosfaderani, J. Zhou, Q. Li, S. S. Sheiko, *Adv. Mater.* **2015**, *27*, 6899.
- [19] X. Ding, J. Gao, Z. Wang, H. Awada, Y. Wang, *Biomaterials* **2016**, *111*, 80.
- [20] R. S. Smith, T. J. Smith, T. M. Bliden, R. P. Phipps, *Am. J. Pathol.* **1997**, *151*, 317.
- [21] J. Arista-Nasr, M. Gonzalez-Romo, C. Keirns, J. Larriva-Sahd, *Arch. Pathol. lab. Med.* **1993**, *117*, 812.
- [22] a) L. Sun, M. Wang, S. Chen, B. Sun, Y. Guo, C. He, X. Mo, B. Zhu, Z. You, *Acta Biomater.* **2019**, *85*, 310; b) Y. Lu, L. Li, Y. Zhu, X. Wang, M. Li, Z. Lin, X. Hu, Y. Zhang, Q. Yin, H. Xia, C. Mao, *ACS Appl. Mater. Interfaces* **2018**, *10*, 127.